

Synthesis and application of CuO-TiO₂ hybrid nanostructures as Photocatalyst for degradation of p-nitrophenol in wastewater

Nianping Chi*, Yishen Wang

School of Municipal and Geomatics Engineering, Hunan City University, Hunan Province Engineering & Technology Research Center for Rural Water Quality Safety, Yiyang, Hunan 413000, China

*E-mail: cnp2022zjgsdx@163.com

Received: 24 July 2022 / Accepted: 30 August 2022 / Published: 10 September 2022

The synthesis of CuO-TiO₂ hybrid nanostructures using the sol-gel method, as well as their characterization as photocatalysts for photodegradation of p-nitrophenol (PNP) in industrial wastewater under sunlight irradiation, were presented in this paper. According to SEM and XRD investigations, the CuO-TiO₂ hybrid nanostructure had a mixture of monoclinic structure CuO and anatase phase TiO₂, indicating that the CuO-TiO₂ hybrid nanostructure was successfully synthesised using the sol-gel method. Optical band gap values for CuO, TiO₂, and CuO-TiO₂ were determined to be 1.64, 3.02, and 2.10 eV, respectively. Electrochemical tests revealed that CuO-TiO₂ has a longer electron lifetime, a higher separation efficiency, and a faster diffusion rate. After 75, 65, and 50 minutes of sunshine irradiation, full elimination of 200 mL of 10 mg/l PNP was obtained employing the photocatalytic activity of TiO₂, CuO, and CuO-TiO₂, respectively. These findings support CuO-high TiO₂'s photocatalytic activity when exposed to sunlight, owing to the synergistic effect of CuO and TiO₂ in forming a CuO-TiO₂ heterojunction with efficient separation of photo-generated electrons and holes, which improves electron transport. After 35, 90, and 150 minutes of UV irradiation, 100% treatment of 5, 30, and 100 mg/L of PNP was obtained, respectively. The CuO-practical TiO₂'s photocatalytic removal capacity was tested for degradation of a 200 mL 5 mg/L PNP solution generated from genuine industrial wastewater, demonstrating CuO-efficient TiO₂'s photocatalytic activity for PNP removal from real industrial wastewater.

Keywords: Photodegradation; CuO-TiO₂ hybrid; Sol-gel; P-nitrophenol; Phenolic compounds; Industrial wastewater

1. INTRODUCTION

P-nitrophenol (PNP), commonly known as 4-nitrophenol or 4-hydroxynitrobenzene, is a phenolic molecule with a nitro group on the benzene ring opposite the hydroxyl group [1, 2]. It's

divided into nitrophenols, which are organic chemicals [3, 4]. PNP is a common environmental pollutant due to its widespread use in the production of pharmaceuticals, fungicides, insecticides, and dyes, as well as in the darkening of leather [5, 6]. Agrochemicals, explosives, and plasticizers are the most common uses. Humans suffering from acute (short-term) inhalation or ingestion of PNP experience headaches, sleepiness, and nausea. Contact with the skin and eyes might cause serious irritation. Ingestion is poisonous, and skin contact is moderately hazardous [7, 8]. It interacts with blood late and creates methaemoglobin, which causes methemoglobinemia, which can result in cyanosis, disorientation, and coma [9, 10].

PNP and its derivatives, as a result, are prevalent contaminants in pharmaceutical and chemical industry wastewaters [11, 12]. Because of these substantial environmental and biological issues, treating phenolic-contaminated wastewater is a major economic and environmental challenge [13]. Thus, numerous studies have been performed to degrade PNP pollutants in wastewaters through electrocoagulation [14], Fenton and electro-Fenton [15, 16], adsorption [17], biodegradation in a sequencing batch reactor [18, 19], electrochemical oxidation [20], and photocatalysis [21-27]. However, a complete degradation has not been achieved using these treatment techniques because of the formation of intermediate degradation products which display a much higher toxicity [28, 29]. However, photocatalytic oxidation, as a very powerful purification technique can destroy phenolic molecules in aquatic media [30-32]. This technique shows some advantages over other existing methods such as requiring a simple reactor, no secondary pollution left by the degraded organic substances, and being able to be reprocessed in an ecofriendly approach [33, 34].

This research described the preparation of CuO-TiO₂ hybrid nanostructures using the sol-gel method, as well as the evaluation of structural, optical, and electrochemical properties, as well as their application as photocatalysts for the photodegradation of PNP, an emerging phenolic pollutant in industrial wastewater, under sunlight irradiation.

2. EXPERIMENT

2.1. Synthesis of photocatalysts

A sol-gel method was used for synthesis of photocatalysts [35]. Then, 1g of Tetrabutyl titanate (TBOT, 97%, Sigma-Aldrich) and 1g of cetyltrimethylammonium bromide (CTAB, 95%, Sigma-Aldrich) were ultrasonically added to 150 mL of ethanol. The ultrasonication was continued for 10 minutes and followed by magnetic stirring for 20 minutes to achieve a transparent solution. Then, under magnetic stirring for 40 minutes, Cu(NO₃)₂ 5H₂O (98%, Sigma-Aldrich) was added to the resultant translucent solution. After aging for 10 hours at room temperature, the mixture was dried for 8 hours at 100 °C. The sample was heated in an oven at 400 °C for 5 hours to calcinate the product and eliminates the organic material, resulting in a CuO-TiO₂ hybrid nanostructure. Pure TiO₂ was synthesized without Cu(NO₃)₂ 5H₂O, and pure CuO was synthesized without Tetrabutyl titanate using the same technique.

2.2. Photodegradation measurements

CuO, TiO₂, and CuO-TiO₂ hybrid nanostructure photodegradation studies for PNP treatment were carried out in a Pyrex flask type reactor with sunshine as a light source. 0.5 g of produced photocatalysts was combined in 200 mL of PNP solutions with magnetic stirring for PNP treatment. The mixture was magnetically agitated in the dark for 30 minutes before the photodegradation measurements were taken in the presence of sunlight to achieve the desorbance-absorbance balance. The stable mixture was then exposed to sunlight for a photocatalytic reaction while being stirred magnetically. To remove photocatalyst particles from the degraded PNP samples, they were centrifuged for 5 minutes at 1000 rpm. Afterwards, the recorded absorption spectrum of degraded PNP using a UV–visible spectrophotometer (UV2500PC; Shimadzu Corp., Japan) at $\lambda=400$ nm was utilized to determine the removal efficiency by the following equation [36, 37]:

$$\text{Removal efficiency (\%)} = \frac{C_0 - C_t}{C_0} \times 100 \quad (1)$$

Where C_0 is the initial concentration of PNP and C_t is the concentration of PNP after photodegradation prose at time t (min).

2.3. Characterizations

The structural and morphological analyses were performed using an X-ray diffractometer (XRD; Siemens D500 diffractometer) and a scanning electron microscope (HILIPS XL30/TMP, the Netherlands). In air at room temperature, UV–Vis absorption spectra (UV2500PC spectrophotometer; Shimadzu Corp., Japan) were obtained in the wavelength range of 300 to 800 nm. Electrochemical impedance spectroscopy (EIS) experiments were carried out on an electrochemistry workstation (CHI 660E, Chenhua Technology Co., Ltd., Shanghai, China) with a three-electrode system consisting of photocatalysts modified ITO electrode as the working electrode, platinum wire as the counter electrode, and an Ag/AgCl electrode as the reference electrode. EIS studies were conducted in a 5 mM K₃[Fe(CN)₆]/K₄[Fe(CN)₆] ($\geq 99.0\%$, Sigma-Aldrich) solution containing 0.1 M KCl (99.0%, Merck, Germany) solution at frequencies ranging from 10⁻⁵ to 10² kHz with a 5 mV amplitude.

3. RESULTS AND DISCUSSION

3.1. SEM and XRD analyses

SEM images of CuO, TiO₂, and CuO-TiO₂ are shown in Figure 1. CuO SEM pictures show small irregular nanoparticles with an average diameter of 70nm that are strongly agglomerated, as seen in Figure 1a. Figure 1b exhibits TiO₂ nanoparticles with an average size of 120nm that were produced in irregular forms. Figure 1c shows that the morphology of the CuO-TiO₂ hybrid nanostructure contains block-like crystals that are grown in rectangular shaped crystalline, indicating a rougher and porous surface with more active sites [38-40], and thus an increased effective surface area for improved photocatalytic performance [41, 42].

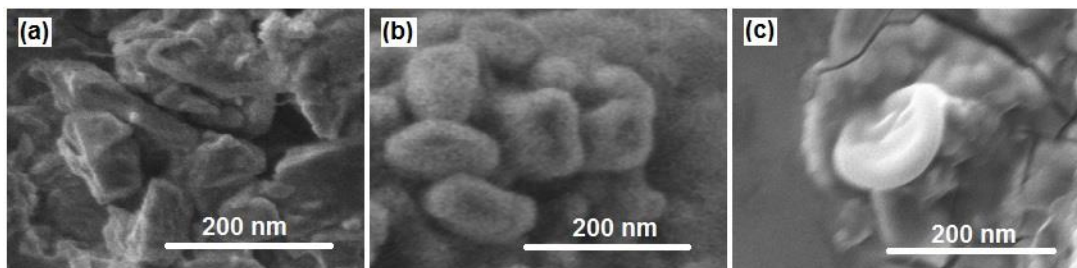


Figure 1. SEM images of (a) CuO, (b) TiO₂ and (c) CuO-TiO₂.

CuO, TiO₂ and CuO-TiO₂ XRD patterns are shown in Figure 2. CuO's XRD pattern reveals characteristic peaks at 32.21°, 33.33°, 38.43°, 48.65°, 53.54°, 61.54°, 65.98°, and 75.17°, corresponding to (110), ($\bar{1}11$), (111), (202), (020), ($\bar{1}13$), (311) and (222) planes, respectively, which are attributed to monoclinic structure CuO. (JCPDS card no. 72-0629) [43-45]. Strong diffraction peaks of (101), (004), (200), (105), (211), (213), (116), (220), and (115) planes are situated at about 25.21°, 36.93°, 47.81°, 53.71°, 54.80°, 62.50°, 68.81°, 69.98°, and 75.01°, respectively, and correspond to TiO₂'s anatase phase (JCPDS card no. 21-1272) [46-48]. As shown in the XRD pattern of CuO-TiO₂, diffraction peaks of ($\bar{1}11$) and (111) planes related to the monoclinic structure of CuO, and diffraction peaks of (101), (200), (105) and (213) planes related to the anatase phase of TiO₂, indicate the synthesis of CuO-TiO₂ hybrid nanostructure using the sol-gel method.

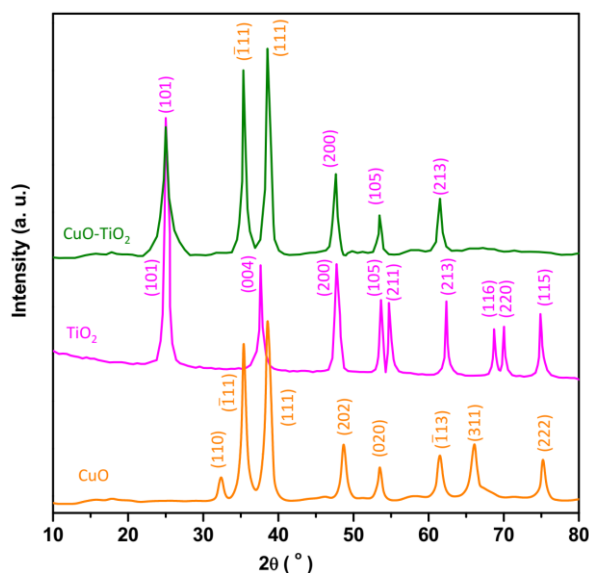


Figure 2. XRD patterns of CuO, TiO₂ and CuO-TiO₂.

3.2. Optical analyses

Figure 3a shows the optical absorbance spectra of CuO, TiO₂, and CuO-TiO₂. The absorbance spectra of anatase TiO₂ show significant absorption in the UV area and low absorption in the visible

region, as shown in the diagram. The absorption edge is at 378 nm, which is associated with electron transport from TiO₂'s valence band to its conduction band [49-51]. It means that pure TiO₂ nanoparticles are UV light active. Pure CuO nanoparticle absorbance spectra reveal a high and broad range of light absorption up to 800 nm, indicating a significant and active absorption of light in the visible region [52, 53]. CuO-TiO₂ has a broad range of absorption as well as the maximum optical absorption when compared to TiO₂ nanoparticles, which can be attributed to the hybrid nanostructured CuO-TiO₂ and its high surface roughness and porosity. Using absorbance spectra and the following equation, the band gap energies (E_g) of the samples were obtained [54-56]:

$$(\alpha h\nu)^{1/2} = A(h\nu - E) \quad (2)$$

Where α is absorption coefficient, $h\nu$ reflects the photon energy, and A is the proportionality parameter. Extrapolating the Tauc plots as linear sections of the curves until they intersect the x-axis in Figure 3b results the E_g values of samples. As seen, the E_g values of CuO, TiO₂ and CuO-TiO₂ are determined ~1.64, 3.02 and 2.10 eV, respectively. It is found that the addition of CuO in the TiO₂ structure decreases the band gap energy of CuO-TiO₂ toward TiO₂ which promotes the visible absorption of TiO₂ and its application in sunlight.

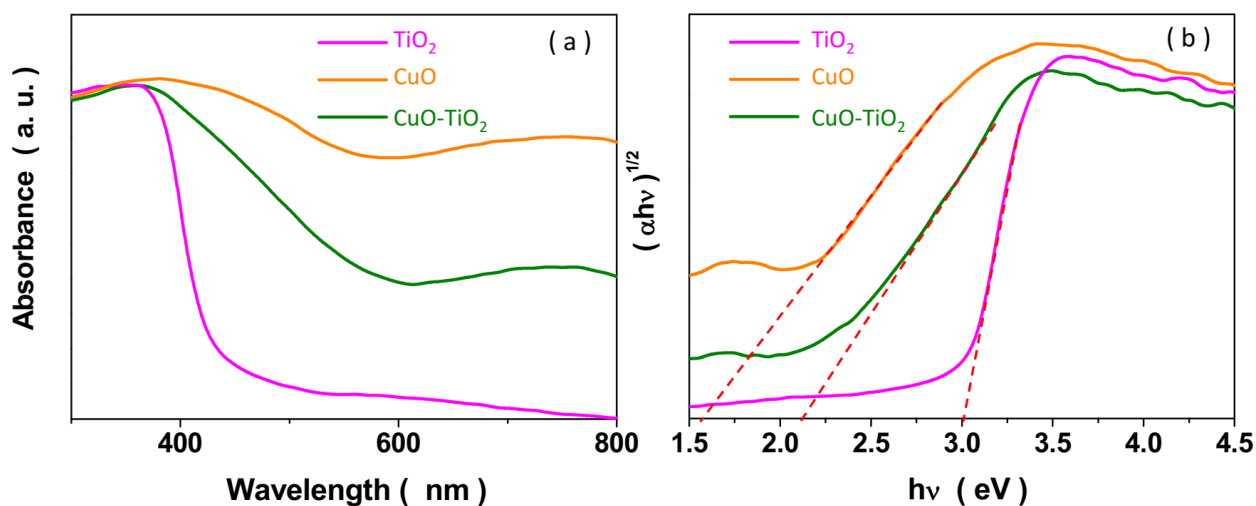


Figure 3. (a) The optical absorbance spectra of, and (b) Tauc plots.

3.3. Electrochemical impedance spectroscopy analyses

The charge transfer pathway was investigated using EIS analysis. The EIS Nyquist and bode plots of TiO₂, CuO, and CuO-TiO₂ under solar light irradiation are shown in Figures 4a and 4b. Figure 4a shows that all electrodes have semicircles in the high frequency band. The charge transfer resistance is represented by the diameter of the semicircle extrapolated in the Nyquist diagram (R_{ct}) [57, 58]. The semicircle with the smallest diameter belongs to the CuO-TiO₂ sample, meaning that it has the lowest charge transfer resistance and the highest separation efficiency of photo-excited electrons and holes, both of which are directly related to the surface area and heterostructured CuO-TiO₂ [59, 60]. The

values of the distinct elements in equivalent electrical circuit models were analyzed using EIS data, as shown in Figure 4a, which includes R_s , which represents the magnitude of the solution resistance, R_{ct} , which represents the solution resistance and charge transfer resistance, CPE, which represents the double layer capacitance, and R_w , which represents the Warburg impedance [61]. R_{ct} usually relates to the photocatalytic kinetics and the smaller value in CuO-TiO₂ represents more efficient charge carrier transfer and a faster redox reaction rate. Therefore, it can be deduced that the CuO-TiO₂ possesses preferable charge transfer efficiency and photocatalytic activity [62]. As seen in Nyquist Plots, there is a straight line inclined at 45° at the low frequency region which corresponds to the R_w because of diffusion controlled of ions in the electrolyte and it describes the mass transport of the electroactive that may be limiting the electron transfer process [63, 64]. In addition, the displayed Bode plots in Figures 4b exhibit the peak frequency (f_{max}) of CuO-TiO₂ toward pure CuO and TiO₂ is shifted to low frequency. Electron lifetime (τ_e) can be determined as $\tau_e = 1 / (2\pi f_{max})$ [65, 66], which indicates that f_{max} is inversely related to the lifetime of electrons. Therefore, the lower f_{max} of CuO-TiO₂ reflects the longer electron lifetime and great separation efficiency and faster diffusion rate in CuO-TiO₂ [67, 68].

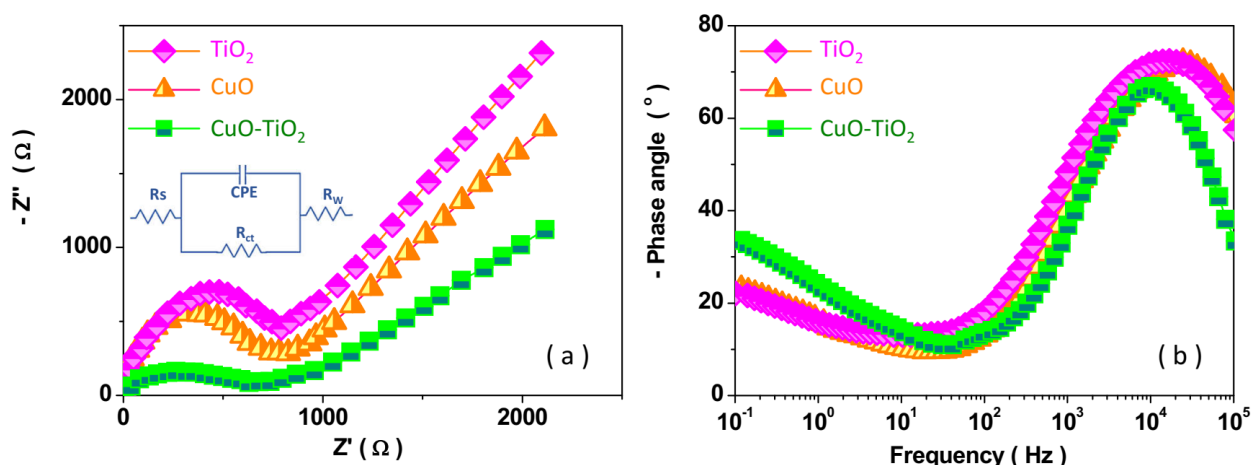


Figure 4. (a) EIS Nyquist and (b) bode plots of TiO₂, CuO and CuO-TiO₂ under sun light irradiation.

Table 1. The obtained parameters by fitting the EIS spectra with the equivalent circuit.

Sample	R_s (Ω)	R_{ct} ($k\Omega$)	CPE (μF)	R_w (Ω)
CuO	5.15	1.15	0.5	1800
TiO ₂	4.22	1.00	15	2400
CuO-TiO ₂	4.02	0.29	0.98	620

3.4. Photodegradation analyses

Figure 5 shows the photocatalytic removal effectiveness of TiO_2 , CuO , and CuO-TiO_2 for the treatment of 200 mL of 10 mg/L PNP solution under sunlight irradiation, as well as the removal efficiency of the control sample (without photocatalyst). After 90 minutes of sunshine irradiation, the removal efficiencies of the control sample are negligible (0.91%), while the photocatalytic removal efficiencies of TiO_2 , CuO , and CuO-TiO_2 are 12.7 %, 21.6 %, and 41.5 %, respectively, after 10 minutes of sunlight irradiation. Furthermore, using the photocatalytic activity of TiO_2 , CuO , and CuO-TiO_2 , 100% elimination of PNP is obtained after 75, 65, and 50 minutes of sunshine irradiation, respectively. These results confirm the great photocatalytic activity of TiO_2 and CuO-TiO_2 under sunlight irradiation and demonstrate more efficient photo-generated electron-hole separation and faster charge transfer of CuO-TiO_2 than that of CuO and TiO_2 which shows good agreement with the XRD, SEM, EIS, and optical analyses. In CuO-TiO_2 , the conduction band (CB) of CuO is more negative than that of TiO_2 . Due to the difference in potential and high separation efficiency of photo-generated electrons and holes, photo-excited electrons have an attraction to transfer from CuO CB to TiO_2 CB, which enhances phenolic pollutant destruction processes. The valence band (VB) of TiO_2 is, on the other hand, more positive than that of CuO , thus the holes produced undergo oxidation reactions with water, producing proton and intermediate intermediates [69, 70]. This results in the accumulation of photogenerated holes and electrons at the VB of CuO and the CB of TiO_2 , respectively. Therefore, the recombination rate of photogenerated holes and electrons in the CuO-TiO_2 is substantially decreased toward the pure CuO and TiO_2 [71, 72]. Accordingly, the photogenerated holes in VB of CuO can promote the reaction to produce hydroxyl radical ($\cdot\text{OH}$), and photogenerated electrons CB of TiO_2 can be transferred to the adsorbed oxygen for the formation of superoxide anion radical ($\cdot\text{O}_2^-$). $\cdot\text{O}_2^-$ and $\cdot\text{OH}$ are strong oxidants that help to the effective oxidation of PNP [73, 74].

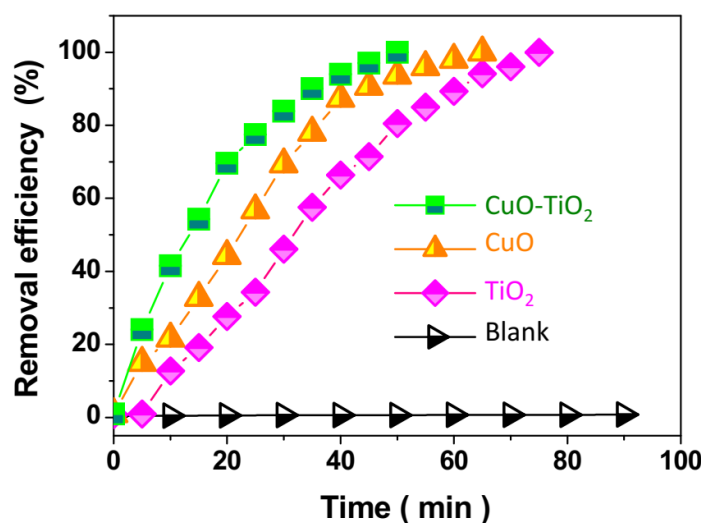


Figure 5. The removal efficiency of control sample (without photocatalyst), and photocatalytic removal efficiency of TiO_2 , CuO and CuO-TiO_2 for the treatment of 200 ml of 10 mg/L PNP solution under sunlight irradiation

Figure 6 illustrates the results of CuO-TiO₂ removal efficiency for varied PNP concentrations treated under sunlight irradiation. After 35, 50, 90, and 150 minutes of UV irradiation, 100 percent treatment of 5, 10, 30, and 100 mg/L of PNP is produced, accordingly. As the starting PNP concentration is increased, the removal efficiency decreases, as shown [75, 76]. Table 2 compares our findings to the photocatalytic activity of photocatalysts reported in the literature for the treatment of PNP. CuO-TiO₂ has a high photocatalytic removal efficiency due to the synergistic impact of CuO and TiO₂ in the production of a CuO-TiO₂ heterojunction with efficient separation of photo-generated electrons and holes, which improves electron transport [71, 77].

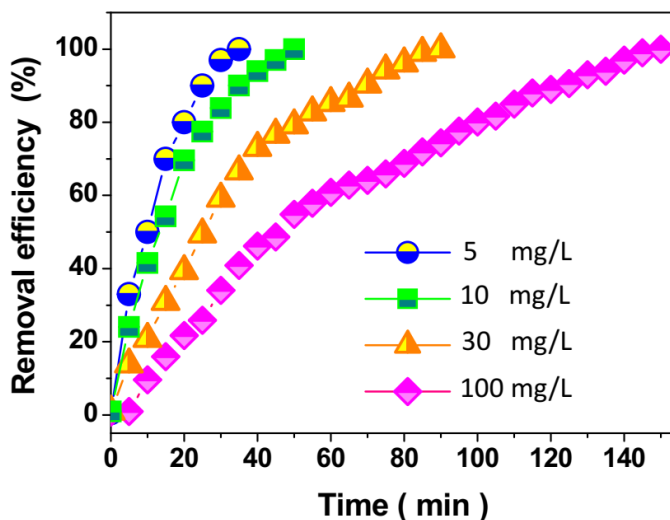


Figure 6. Removal efficiency of CuO-TiO₂ for treatment 200 mL of various PNP concentrations (5, 10, 30 and 100 mg/L) under sunlight irradiation.

Table 2. Comparison between the photocatalytic activity of CuO-TiO₂ and other photocatalysts reported in the literatures for treatment of PNP.

Photocatalyst	PNP content (mg/l)	Light source	Degradation time (minute)	Removal efficiency (%)	Ref.
TiO ₂	5	UV	120	88	[21]
rGO/ZrO ₂	10	UV	100	>90	[25]
Pt/BiOBr-0.27	10	visible	90	85.3	[26]
TiO ₂	14	UV	120	90%	[24]
SnO ₂ -rGO	20	UV	90	95.6	[22]
Carbon quantum dots/TiO ₂	30	UV	150	96	[23]
CuO-TiO ₂	5	UV	35	100	Present study
	10		50	100	
	30		90	100	
	100		150	100	

3.5. PNP treatment of actual industrial wastewater

The practical photocatalytic removal ability of 200 mL of 5 mg/L PNP solution was generated from genuine industrial effluent (PNP-1) obtained from Tairui Fine Chemical Co., Ltd. (Tianjin, China). The control sample was made with deionized water for comparison (PNP-2). Figure 7 demonstrates that under solar irradiation, full photocatalytic elimination of PNP-1 and PNP-2 takes 50 and 35 minutes, respectively. The prolonged time for complete treatment of PNP-1 made from real industrial wastewater is due to the examined wastewater sample containing a large number of phenolic compounds and dyes, which cause pollutants to adsorb on the CuO-TiO₂ surface and slow down photocatalytic reactions. As a result, these data show that CuO-TiO₂ has a high photocatalytic activity for the treatment of PNP in genuine industrial effluent.

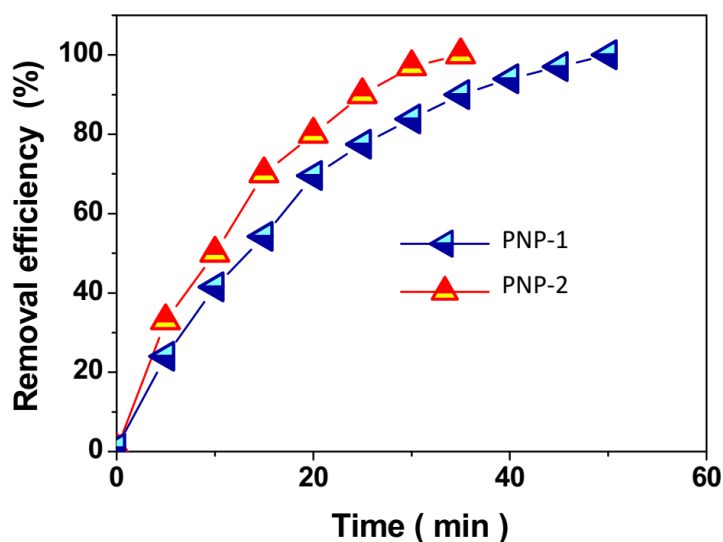


Figure 7. The photocatalytic removal ability of CuO-TiO₂ for degradation the 200 mL of 5 mg/L PNP solutions under sunlight irradiation (PNP-1: sample made from actual industrial wastewater, and PNP-2: sample made with deionized water).

4. CONCLUSION

This research focused on the preparation of CuO-TiO₂ hybrid nanostructures using the sol-gel method, as well as the evaluation of structural, optical, and electrochemical properties, as well as their application as photocatalysts for the photodegradation of PNP, an emerging phenolic pollutant in industrial wastewater, under sunlight irradiation. The morphology of the CuO-TiO₂ hybrid nanostructure grew block like crystals with a mixture of monoclinic structure CuO and anatase phase TiO₂, showing that the CuO-TiO₂ hybrid nanostructure was successfully synthesised using the sol-gel method, according to structural studies. Optical investigations revealed that the E_g values of CuO-TiO₂, and CuO-TiO₂ were 1.64, 3.02, and 2.10 eV, respectively, meaning that the addition of CuO in the TiO₂ structure decreased the band gap energy of CuO-TiO₂ toward TiO₂, promoting visible absorption

of TiO₂ and its use in sunlight. According to EIS analyses, the CuO-TiO₂ has a longer electron lifetime, a high separation efficiency, and a faster diffusion rate. After 75, 65, and 50 minutes of sunshine irradiation, full elimination of 200 mL of 10 mg/l PNP was obtained employing the photocatalytic activity of TiO₂, CuO, and CuO-TiO₂, respectively. These findings support CuO-high TiO₂'s photocatalytic activity when exposed to sunlight, owing to the synergistic effect of CuO and TiO₂ in forming a CuO-TiO₂ heterojunction with efficient separation of photo-generated electrons and holes, which improves electron transport. After 35, 90, and 150 minutes of UV irradiation, 100% treatment of 5, 30, and 100 mg/L of PNP was obtained, respectively. The CuO-practical TiO₂'s photocatalytic removal capacity was tested for degradation of a 200 mL 5 mg/L PNP solution generated from genuine industrial wastewater, demonstrating CuO-efficient TiO₂'s photocatalytic activity for PNP removal from real industrial wastewater.

ACKNOWLEDGEMENT

The authors are grateful for the financial support provided by the Natural Science Foundation of Hunan Province (No.2022JJ50263), the College Students' innovation and entrepreneurship training program (S202111527016) and the Scientific Research Funds Project of Hunan Education Department (19B097).

References

1. J. Wei, T. Lu, F. Dong, C. Zhang and Y. Zhang, *Toxicology*, 463 (2021) 152991.
2. Y. Chen, J. Li, J. Lu, M. Ding and Y. Chen, *Polymer Testing*, 108 (2022) 107516.
3. J. Lu, Y. Chen, M. Ding, X. Fan, J. Hu, Y. Chen, J. Li, Z. Li and W. Liu, *Carbohydrate Polymers*, 277 (2022) 118871.
4. H. Karimi-Maleh, R. Darabi, M. Shabani-Nooshabadi, M. Baghayeri, F. Karimi, J. Rouhi, M. Alizadeh, O. Karaman, Y. Vasseghian and C. Karaman, *Food and Chemical Toxicology*, 162 (2022) 112907.
5. S. Kuang, Q. Le, J. Hu, Y. Wang, N. Yu, X. Cao, M. Zhang, Y. Sun, W. Gu and Y. Yang, *Comparative Biochemistry and Physiology Part C: Toxicology & Pharmacology*, 228 (2020) 108638.
6. W. Liu, F. Huang, Y. Liao, J. Zhang, G. Ren, Z. Zhuang, J. Zhen, Z. Lin and C. Wang, *Angewandte Chemie*, 120 (2008) 5701.
7. M.B. Forrester, G.M. Layton and S.M. Varney, *Clinical toxicology*, 58 (2020) 748.
8. W. Liu, J. Zheng, X. Ou, X. Liu, Y. Song, C. Tian, W. Rong, Z. Shi, Z. Dang and Z. Lin, *Environmental science & technology*, 52 (2018) 13336.
9. X. Wang, Y. Zhang, M. Luo, K. Xiao, Q. Wang, Y. Tian, W. Qiu, Y. Xiong, C. Zheng and H. Li, *Science of The Total Environment*, 763 (2021) 144616.
10. T. Gao, C. Li, Y. Zhang, M. Yang, D. Jia, T. Jin, Y. Hou and R. Li, *Tribology International*, 131 (2019) 51.
11. J. Luo, Y. Xu, J. Wang, L. Zhang, X. Jiang and J. Shen, *Journal of Environmental Sciences*, 108 (2021) 134.
12. C. Yu, X. Chen, N. Li, Y. Zhang, S. Li, J. Chen, L. Yao, K. Lin, Y. Lai and X. Deng, *Environmental Science and Pollution Research*, 29 (2022) 18423.
13. F. Yu, Z. Zhu, C. Li, W. Li, R. Liang, S. Yu, Z. Xu, F. Song, Q. Ren and Z. Zhang, *Applied Catalysis B: Environmental*, 314 (2022) 121467.

14. N. Modirshahla, M. Behnajady and S. Mohammadi-Aghdam, *Journal of Hazardous materials*, 154 (2008) 778.
15. L. Feng, J.J. Liu, Z.C. Guo, T.Y. Pan, J.H. Wu, X.H. Li, B.Z. Liu and H.L. Zheng, *Separation and Purification Technology*, 285 (2021)120314.
16. Y.-S. Ma, S.-T. Huang and J.-G. Lin, *Water science and technology*, 42 (2000) 155.
17. L. Feng, X.H. Li, W.C. Lu, Z. Liu, C. Xu, Y. Chen, H.L. Zheng. *International Journal of Biological Macromolecules*, 150 (2020) 617.
18. M.C. Tomei and M.C. Annesini, *Environmental science & technology*, 39 (2005) 5059.
19. Y. Yang, H. Zhu, X. Xu, L. Bao, Y. Wang, H. Lin and C. Zheng, *Microporous and Mesoporous Materials*, 324 (2021) 111289.
20. J.-P. Zou, Y. Chen, S.-S. Liu, Q.-J. Xing, W.-H. Dong, X.-B. Luo, W.-L. Dai, X. Xiao, J.-M. Luo and J. Crittenden, *Water research*, 150 (2019) 330.
21. S.-x. Li, F.-y. Zheng, X.-l. Liu, F. Wu, N.-s. Deng and J.-h. Yang, *Chemosphere*, 61 (2005) 589.
22. Y. Chen, F. Sun, Z. Huang, H. Chen, Z. Zhuang, Z. Pan, J. Long and F. Gu, *Applied Catalysis B: Environmental*, 215 (2017) 8.
23. F. Zheng, Z. Wang, J. Chen and S. Li, *RSC Advances*, 4 (2014) 30605.
24. S. Islam, S.K. Bormon, M. Nadim, K. Hossain, A. Habib and T.S.A. Islam, *American Journal of Analytical Chemistry*, 2014 (2014) 1.
25. S.N. Basahel, M. Mokhtar, E.H. Alsharaeh, T.T. Ali, H.A. Mahmoud and K. Narasimharao, *Nanoscience and Nanotechnology Letters*, 8 (2016) 448.
26. Y. Jia, Y. Yang, Y. Guo, W. Guo, Q. Qin, X. Yang and Y. Guo, *Dalton Transactions*, 44 (2015) 9439.
27. Z. Tasic, V. Gupta and M. Antonijevic, *International Journal of Electrochemical Science*, 9 (2014) 3473.
28. O.A. Osin, T. Yu, X. Cai, Y. Jiang, G. Peng, X. Cheng, R. Li, Y. Qin and S. Lin, *Frontiers in chemistry*, 6 (2018) 192.
29. H. Liu, J. Yang, Y. Jia, Z. Wang, M. Jiang, K. Shen, H. Zhao, Y. Guo, Y. Guo and L. Wang, *Environmental Science & Technology*, 55 (2021) 10734.
30. T. Li, W. Yin, S. Gao, Y. Sun, P. Xu, S. Wu, H. Kong, G. Yang and G. Wei, *Nanomaterials*, 12 (2022) 982.
31. M. Yang, C. Li, Y. Zhang, D. Jia, R. Li, Y. Hou, H. Cao and J. Wang, *Ceramics International*, 45 (2019) 14908.
32. H. Maleh, M. Alizadeh, F. Karimi, M. Baghayeri, L. Fu, J. Rouhi, C. Karaman, O. Karaman and R. Boukherroub, *Chemosphere*, (2021) 132928.
33. S. Kumar, W. Ahlawat, G. Bhanjana, S. Heydarifard, M.M. Nazhad and N. Dilbaghi, *Journal of nanoscience and nanotechnology*, 14 (2014) 1838.
34. J. Liu, T. Li, H. Zhang, W. Zhao, L. Qu, S. Chen and S. Wu, *Materials Today Bio*, 14 (2022) 100243.
35. S. Qin, F. Xin, Y. Liu, X. Yin and W. Ma, *Journal of Colloid and Interface Science*, 356 (2011) 257.
36. Z. Wang, A. He and L. Liu, *International Journal of Electrochemical Science*, 17 (2022) 220645.
37. L. Liu, A. He and X. Yao, *International Journal of Electrochemical Science*, 17 (2022) 220635.
38. H. Savaloni, R. Savari and S. Abbasi, *Current Applied Physics*, 18 (2018) 869.
39. H. Savaloni, E. Khani, R. Savari, F. Chahshouri and F. Placido, *Applied Physics A*, 127 (2021) 1.
40. F. Chen, J. Ma, Y. Zhu, X. Li, H. Yu and Y. Sun, *Journal of Hazardous Materials*, 426 (2022) 128064.

41. F. Chahshouri, H. Savaloni, E. Khani and R. Savari, *Journal of Micromechanics and Microengineering*, 30 (2020) 075001.
42. R. Savari, H. Savaloni, S. Abbasi and F. Placido, *Sensors and Actuators B: Chemical*, 266 (2018) 620.
43. Z. Tan, B. Dong, M. Xing, X. Sun, B. Xi, W. Dai, C. He, Y. Luo and Y. Huang, *Environmental Technology*, (2022) 1.
44. Y. Wang, C. Li, Y. Zhang, M. Yang, B. Li, L. Dong and J. Wang, *International Journal of Precision Engineering and Manufacturing-Green Technology*, 5 (2018) 327.
45. H. Karimi-Maleh, H. Beitollahi, P.S. Kumar, S. Tajik, P.M. Jahani, F. Karimi, C. Karaman, Y. Vasseghian, M. Baghayeri and J. Rouhi, *Food and Chemical Toxicology*, (2022) 112961.
46. Q. Wang, S. Wu, D. Cui, H. Zhou, D. Wu, S. Pan, F. Xu and Z. Wang, *Science of The Total Environment*, 850 (2022) 158034.
47. Q. Wang, H. Sha, S. Cao, B. Zhao, G. Wang and P. Zheng, *Bioresource Technology*, 359 (2022) 127470.
48. M. Yang, C. Li, Y. Zhang, Y. Wang, B. Li, D. Jia, Y. Hou and R. Li, *Applied Thermal Engineering*, 126 (2017) 525.
49. R. Abazari, A.R. Mahjoub and S. Sanati, *Rsc Advances*, 4 (2014) 56406.
50. R. Savari, J. Rouhi, O. Fakhar, S. Kakooei, D. Pourzadeh, O. Jahanbakhsh and S. Shojaei, *Ceramics International*, 47 (2021) 31927.
51. J. Zhang, C. Li, Y. Zhang, M. Yang, D. Jia, G. Liu, Y. Hou, R. Li, N. Zhang and Q. Wu, *Journal of cleaner production*, 193 (2018) 236.
52. M.A. Khan, N. Nayan, Shadiullah, M.K. Ahmad and C.F. Soon, *Nanomaterials*, 10 (2020) 1298.
53. Z. Tan, H. Zhu, X. He, B. Xi, Y. Tian, X. Sun, H. Zhang and Q. Ouche, *Environmental Science and Pollution Research*, (2022) 1.
54. R. López and R. Gómez, *Journal of sol-gel science and technology*, 61 (2012) 1.
55. Y. Qin, B. Xi, X. Sun, H. Zhang, C. Xue and B. Wu, *Frontiers in Bioengineering and Biotechnology*, 10 (2022) 905466.
56. L. Tang, Y. Zhang, C. Li, Z. Zhou, X. Nie, Y. Chen, H. Cao, B. Liu, N. Zhang and Z. Said, *Chinese Journal of Mechanical Engineering*, 35 (2022) 1.
57. Z. Said, S. Arora, S. Farooq, L.S. Sundar, C. Li and A. Allouhi, *Solar Energy Materials and Solar Cells*, 236 (2022) 111504.
58. X. Cui, C. Li, Y. Zhang, Z. Said, S. Debnath, S. Sharma, H.M. Ali, M. Yang, T. Gao and R. Li, *Journal of Manufacturing Processes*, 80 (2022) 273.
59. X. Wang, C. Li, Y. Zhang, H.M. Ali, S. Sharma, R. Li, M. Yang, Z. Said and X. Liu, *Tribology International*, 174 (2022) 107766.
60. H. Karimi-Maleh, C. Karaman, O. Karaman, F. Karimi, Y. Vasseghian, L. Fu, M. Baghayeri, J. Rouhi, P. Senthil Kumar and P.-L. Show, *Journal of Nanostructure in Chemistry*, (2022) 1.
61. A. Mujtaba, N.K. Janjua, T. Yasin and S. Sabahat, *Journal of the Iranian Chemical Society*, 17 (2020) 649.
62. Y. Lin, C. Lu and C. Wei, *Journal of Alloys and Compounds*, 781 (2019) 56.
63. J. Huang, *Electrochimica Acta*, 281 (2018) 170.
64. D. Ge, H. Yuan, J. Xiao and N. Zhu, *Science of The Total Environment*, 679 (2019) 298.
65. L. Wei, P. Wang, Y. Yang, Y. Dong, R. Fan, W. Song, Y. Qiu, Y. Yang and T. Luan, *Thin Solid Films*, 639 (2017) 12.
66. X. Wu, C. Li, Z. Zhou, X. Nie, Y. Chen, Y. Zhang, H. Cao, B. Liu, N. Zhang and Z. Said, *The International Journal of Advanced Manufacturing Technology*, 117 (2021) 2565.
67. Y. Xu, X. Wang, M. Jin, G. Zhou and L. Shui, *Journal of Materials Science*, 55 (2020) 5499.
68. W. Liu, J. Li, J. Zheng, Y. Song, Z. Shi, Z. Lin and L. Chai, *Environmental Science & Technology*, 54 (2020) 11971.

69. T. Trang, L. Tu, T. Man, M. Mathesh, N. Nam and V. Thu, *Composites Part B: Engineering*, 174 (2019) 106969.
70. Y. Wang, X. Wu, J. Liu, Z. Zhai, Z. Yang, J. Xia, S. Deng, X. Qu, H. Zhang and D. Wu, *Journal of Environmental Chemical Engineering*, 10 (2022) 107091.
71. H. Hamad, M.M. Elsenety, W. Sadik, A.-G. El-Demerdash, A. Nashed, A. Mostafa and S. Elyamny, *Scientific Reports*, 12 (2022)
72. T. Gao, C. Li, Y. Wang, X. Liu, Q. An, H.N. Li, Y. Zhang, H. Cao, B. Liu and D. Wang, *Composite Structures*, 286 (2022) 115232.
73. K. Yang, W. Pu, Y. Tan, M. Zhang, C. Yang and J. Zhang, *Materials science in semiconductor processing*, 27 (2014) 777.
74. D. Jia, Y. Zhang, C. Li, M. Yang, T. Gao, Z. Said and S. Sharma, *Tribology International*, 169 (2022) 107461.
75. B. Li, C. Li, Y. Zhang, Y. Wang, D. Jia and M. Yang, *Chinese Journal of Aeronautics*, 29 (2016) 1084.
76. T. Gao, Y. Zhang, C. Li, Y. Wang, Y. Chen, Q. An, S. Zhang, H.N. Li, H. Cao and H.M. Ali, *Frontiers of Mechanical Engineering*, 17 (2022) 1.
77. Y. Li, Q. Bai, Y. Guan, P. Zhang, R. Shen, L. Lu, H. Liu, X. Yuan, X. Miao and W. Han, *Nuclear Fusion*, 62 (2022) 076023.

© 2022 The Authors. Published by ESG (www.electrochemsci.org). This article is an open access article distributed under the terms and conditions of the Creative Commons Attribution license (<http://creativecommons.org/licenses/by/4.0/>).